ELSEVIER

Computers & Geosciences 32 (2006) 1420–1431

COMPUTERS & GEOSCIENCES

www.elsevier.com/locate/cageo

# Analyzing rock magnetic measurements: The RockMagAnalyzer 1.0 software

R. Leonhardt

*Department for Earth and Environmental Sciences, Ludwig-Maximilians-Universität, München, Germany*

Received 13 June 2005; received in revised form 28 October 2005; accepted 9 January 2006

**Abstract**

The ROCKMAG ANALYZER is a software to determine rock magnetic parameters from a broad variety of rock magnetic measurements. This software was particularly designed to visualize and evaluate data from isothermal remanent magnetization acquisition, coercivity curves, hysteresis loops and/or thermomagnetic curves. Various standard and non-standard rock magnetic parameters are calculated from these curves, thus, accelerating and simplifying the quantitative analysis of the measured data. View options like plotting derivatives, para-/diamagnetic correction, etc. further enhance the data analysis. Procedures for smoothing and data fitting by mathematical functions are implemented. Isothermal remanent magnetization acquisition and coercivity curves can be fitted by log-Gaussian functions and hysteresis loops by hyperbolic basic functions. Curie temperature estimation from thermomagnetic curves is supported by two different automated approaches: a second derivative method and a extrapolation method. A number of additional diagrams provide composite plots of parameters obtained by different measurements, like the Day plot and the Henkel plot.

The ROCKMAG ANALYZER was designed for the output file format of the Variable Field Translation Balance (MM VFTB). It also supports data from the PM VSM/AGFM. The ROCKMAG ANALYZER requires Win95/98/ME/2k/XP and is available at "http://www.geophysik.uni-muenchen.de/research/paleomagnetism/".


*Keywords:* Rock magnetism; Hysteresis; Isothermal magnetization; Curie temperature; Variable field translation balance

## 1. Introduction

The analysis of rock magnetic measurements is an important part of characterizing magnetic materials in paleomagnetic, mineralogical, climatological, and environmental studies. In principal, such measurements are aimed to identify grain size, domain state, composition, concentration, stress-state, and other mineralogical properties of the magnetic mineral or of mixtures of magnetic phases in those materials. Several sophisticated instruments are capable of performing the most commonly used rock magnetic measurements. Such instruments are the Variable Field Translation Balance (MM VFTB), the Vibrating Sample Magnetometer (Princeton Measurement Ltd. VSM), and the Alternating Gradient Force Magnetometer (Princeton Measurement Ltd. AGFM). Basically, two groups of measurements are supported by those instruments: pure remanence measurements, like isothermal remanent magnetization (IRM) acquisition and associated backfield curves, as well as hysteresis loops and thermomagnetic measurements. For the

*E-mail address:* leon@geophysik.uni-muenchen.de.

0098-3004/$ - see front matter © 2006 Elsevier Ltd. All rights reserved.
doi:10.1016/j.cageo.2006.01.006

analysis of such data, however, various different tools are available, and mostly it is not stated how magnetic parameters were calculated from the related measurements. For example, Curie temperatures are frequently used to identify magnetic minerals but in most cases information about the method used for estimation is missing.

Here a software, the ROCKMAG ANALYZER, for the analysis of rock magnetic measurements is presented and in the following the different methods used for determining parameters from the measurements are outlined. The ROCKMAG ANALYZER is particularly designed for the analysis of rock magnetic measurements from the MM VFTB. However, it also supports data formats of the PM VSM and the PM AGFM. Various standard and non-standard rock magnetic parameters are calculated. Furthermore, procedures for smoothing and data fitting using mathematical functions are implemented. Analysis of data is accompanied by related graphs like hysteresis loops and thermomagnetic curves, IRM curves and coercivity curves, as well as a number of additional plots e.g. for the combined analysis of IRM and backfield curves.

The ROCKMAG ANALYZER is freeware and can be downloaded at "http://www.geophysik.uni-muenchen.de/research/paleomagnetism/".

## 2. Program handling

### 2.1. File formats

The ROCKMAG ANALYZER is capable of opening output data files from the MM VFTB. Furthermore, data files from the Princeton Measurement Ltd. VSM/AGFM (model 2900) are supported. Prerequisite for the correct visualization of the data are the following file extensions: *.irm for IRM acquisition curves, *.coe for isothermal backfield measurements, *.hys for hysteresis loops and *.rmp for thermomagnetic curves. By opening one of these files in a directory, e.g. the "example1.coe" file, all other existing measurement files (IRM, HYS and RMP) with the same file name will be opened as well. The file name is assumed to represent the sample name. The supported data format from the MM VFTB is shown in Table 1.

IRM, backfield and hysteresis files may contain several sets of measurements obtained, for example, at different temperatures.

### 2.2. User interface

The *Main window* after opening a set of VFTB data is shown in Fig. 1. This window is split into two sections: The graph with the selected plot is

Table 1
Supported data format

| Name: Example 1 weight: 146.8 mg | | | | | File Header |
|---|---|---|---|---|---|
| Set 1: Field (Oe) | Mag/E-3 emu (g) | Std dev/E-3 emu (g) | Temp °C | Time (s) | Set definition Data Header |
| 37.7 | 5.872360052e−004 | 4.895405486e−004 | 24 | 0 | |
| 70.9 | 2.507481437e−003 | 4.170446873e−004 | 24 | 0 | |
| 105.4 | 4.650360637e−003 | 4.203251927e−004 | 24 | 0 | |
| 210 | 1.290038184e−002 | 4.054529164e−004 | 24 | 0 | |
| 349 | 2.227562346e−002 | 4.082850199e−004 | 24 | 0 | |
| 699 | 3.430062417e−002 | 3.91717597e−004 | 24 | 0 | |
| 1051 | 3.98135714e−002 | 4.102903746e−004 | 24 | 0 | Data |
| 1752 | 4.643890076e−002 | 3.926859381e−004 | 24 | 0 | |
| 2840 | 5.093442342e−002 | 4.166532017e−004 | 24 | 0 | |
| 4220 | 5.554256764e−002 | 3.575008103e−004 | 24 | 0 | |
| 5590 | 5.955917149e−002 | 3.596839777e−004 | 24 | 0 | |
| 7270 | 6.382053612e−002 | 2.972939182e−004 | 24 | 0 | |
| 9150 | 6.766503055e−002 | 3.495826645e−004 | 24 | 0 | |

Data format supported by the ROCKMAG ANALYZER software. Shown is the "example1.irm" file containing IRM acquisition data. Data files without the standard-deviation column (3rd) or without standard-deviation and time columns can also be opened. CGS units are automatically converted into SI-units. Up to 4 multiple data sets within one file, separated by Set definitions, are identified and the set used for analysis can be selected in the program. Analysis of time-dependent measurements is not supported by the ROCKMAG ANALYZER.

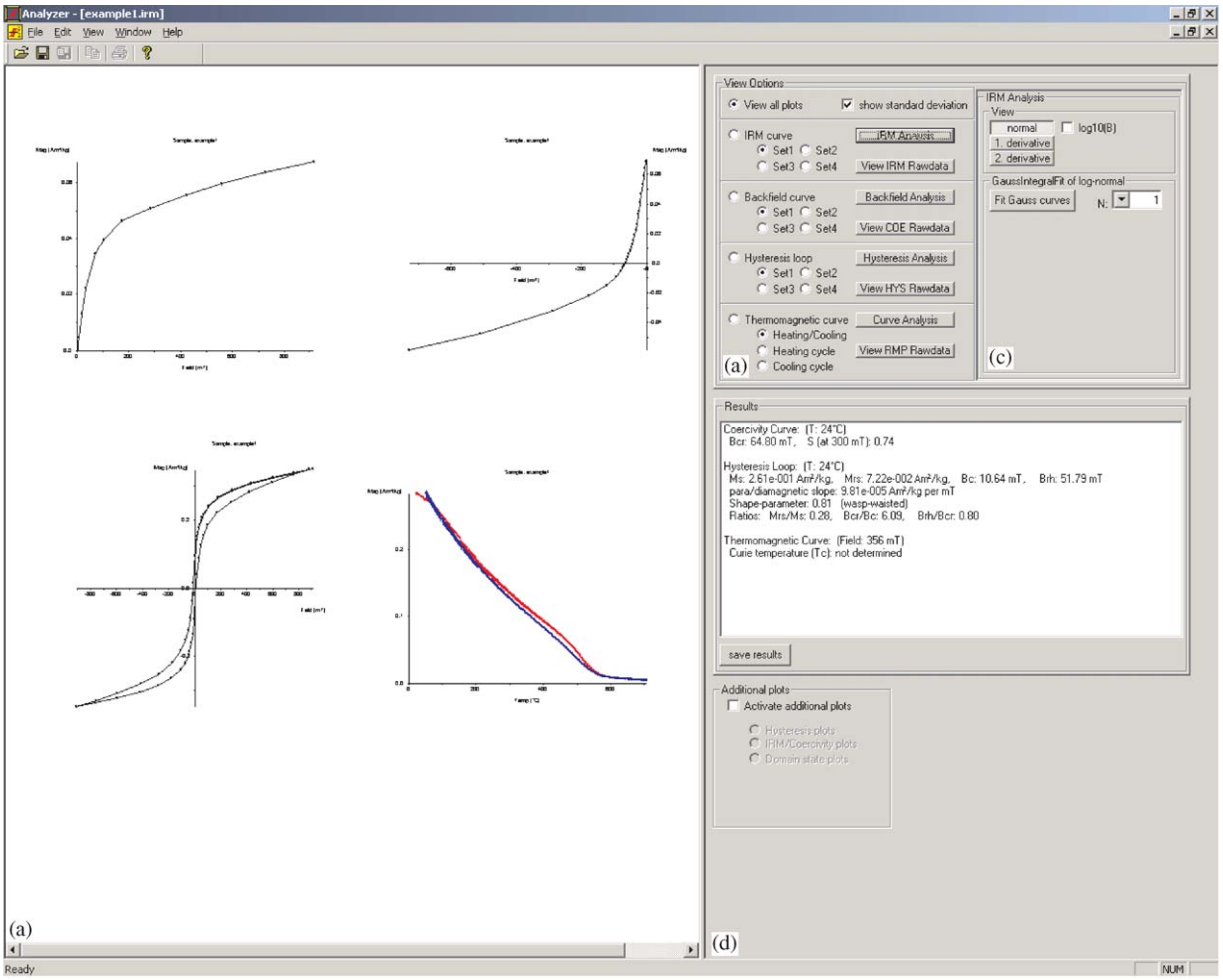


Fig. 1. *Main view* of the ROCKMAG ANALYZER. In (a) currently selected set of plots is shown. By changing view options (b) either all plots or an enlarged view of individual measurements can be selected. If more than one IRM acquisition, coercivity curve or hysteresis loop was measured in one run (e.g. at different temperatures) the desired data set for calculation can be selected. Furthermore, it is possible to open raw-data file using an external text editor and to activate advanced analysis options. Results for rock magnetic parameters calculated from measured curves are printed in list box (c). Additional plots are available in (d). If advanced analysis is selected, e.g. IRM analysis, an inset (e) is enabled.

displayed on the left side (Fig. 1a). The form view on the right-hand side contains view selections, results and several options regarding data analysis.

In the *View Options* field (Fig. 1b) the displayed plot and, if more than one set was measured, the active data set, which is then used for calculations can be selected. For thermomagnetic curves either the heating cycle, the cooling cycle, or both can be shown. If the display of both, heating and cooling cycle is selected only the heating cycle is used for further analysis. Raw-data files can be opened in NOTEPAD using the *View Rawdata* button and further analysis options can be enabled with the *IRM,COE,HYS,RMP Analysis* buttons.

The *Results* field (Fig. 1c) contains relevant measurement settings and the rock magnetic parameters as calculated by the software. All displayed results are written or appended (if the selected file already exists) to a tab-delimited text file by clicking on the *Save Results* button.

*Additional Plots* (Fig. 1d) can be displayed by enabling the *Activate additional plots* check box. This option disables the standard view options and provides the possibility to show further plots of hysteresis, IRM/coercivity as well as hysteresis/coercivity parameters.

If one of the analysis buttons is used, an additional field related to either IRM, COE, HYS

or RMP *Analysis* is shown (Fig. 1e). Here, several additional view options as well as advanced analysis options are provided.

Selected plots can be transferred to other applications using copy/paste commands or saved as a vector-type graphic to an enhanced metafile using the *Save plot* option.

## 3. Standard analysis

After opening data files with the ROCKMAG ANALYZER, a series of analyzes is automatically conducted on backfield (COE) and hysteresis (HYS) measurements. Isothermal (IRM) and thermomagnetic (RMP) curves are not analyzed automatically, but can be evaluated using advanced analyzes options (see below). A technical description of the methods used for the determination of rock magnetic parameters from COE and HYS is given below. Results from the analysis are shown in the *Results* field of the form view Fig. 1c.

### 3.1. Coercivity curve

From the backfield curve two parameters are determined, the remanence coercivity $B_{cr}$ and, by default, the $S_{300}$ parameter, which corresponds to $(1-(M_{-300\,mT}/M_{rs}))/2$ (Bloemendal et al., 1992). $B_{cr}$ is determined by finding the intersection of the linear interpolated measurement data with the axis representing zero-magnetization. For the calculation of $S_{300}$, the initial magnetization is used as an approximation of the saturation remanence ($M_{rs}$) and the magnetization at $-300\,mT$ ($M_{-300\,mT}$) is determined by linear interpolation of measured data.

### 3.2. Hysteresis loop

Hysteresis measurements conducted with the MM VFTB always begin at zero-field and then continue at predefined field steps up to the maximum applied field. After the maximum field is reached, the major hysteresis loop is measured at the same field steps. Only this major loop of the hysteresis is analyzed by

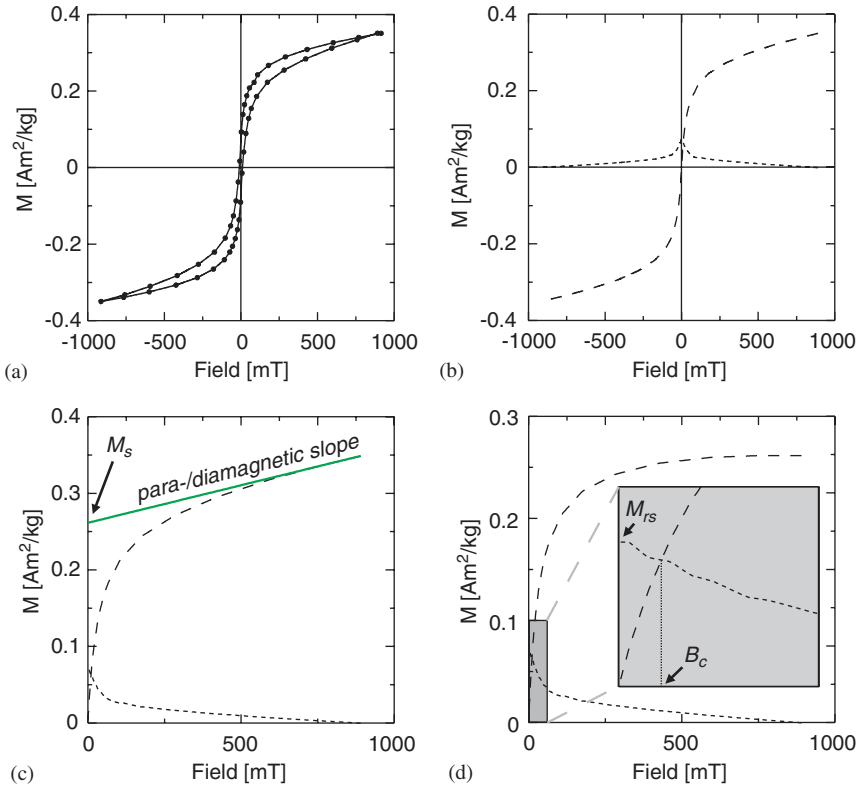


Fig. 2. Determination of hysteresis parameters: (a) Original data (circles) and linear interpolated curve; (b) mean curve (dashed) and difference curve (dotted) of lower and upper hysteresis branches; (c) mean and difference curve after averaging symmetrical parts; (d) mean and difference curve after para-diamagnetic correction using slope of the linear fit in (c).

standard analyzes. The actual field values for each field step are measured and commonly differ slightly for the individual branches of the major loop. To account for this difference, the mean of the actual fields is determined for each field step and rounded to an accuracy of 1 mT. For each branch and each field step of the hysteresis loop, the magnetization is calculated at this mean field value by linear interpolation. As the mean field values differ only slightly from the actual field values, a linear interpolation is justified and the resulting error is negligible. Original data and the corresponding interpolated curve are shown in Fig. 2a. After interpolation, the mean value of upper and lower branch characterizing the induced part of the loop (hereinafter referred to as mean curve), as well as the half difference between the two branches characterizing the remanent part of the loop (difference curve) are determined (Fig. 2b). Any field offset leading to a deviation of the zero-magnetization crossing of the mean curve is corrected for. Then the symmetrical parts of both mean and difference curve are averaged (Fig. 2c). By default, a linear fit is then determined between the maximum field and 80% of the maximum field. The slope $m_p$ of this linear fit is assumed to represent the para-/diamagnetic contribution. The saturation magnetization $M_s$ is defined by the intersection of the linear fit and the $y$-axis. Using $m_p$, the magnetization values of the hysteresis curve are corrected according to:

$$M_{\text{ferri}}(B) = M(B) - m_p \cdot B. \quad (1)$$

Hysteresis parameter $B_c$ is obtained from the corrected curve (Fig. 2d). The field value of the intersection of mean and difference curve corresponds to $B_c$, the zero-field value of the difference curve is $M_{rs}$. In addition to these standard hysteresis parameters, two other parameters, $\sigma_{Hys}$ and $B_{rh}$ are calculated. The shape parameter $\sigma_{Hys}$ gives a quantitative measure dependent on the shape of the hysteresis loop (Fabian, 2003):

$$\sigma_{Hys} = \log \frac{E_{Hys}}{4 M_s B_c}. \quad (2)$$

$E_{Hys}$ corresponds to the total area between upper and lower branch of the hysteresis loop. Negative values of $\sigma_{Hys}$ indicate pot-bellied, positive values are related to wasp-waisted hysteresis curves. $B_{rh}$ is the median destructive field of the difference curve. In addition, several typically used ratios of hysteresis parameters are printed to the *Results* field.

## 4. Advanced analysis of measurements

The view options for advanced analysis (e.g. *IRM Anaylysis*) activate the analysis field in the *Main view* (Fig. 1e). This inset contains additional analysis options for individual measurements. Possible options for the four measurement procedures are shown in Fig. 3. All analysis frames are subdivided in an upper *View* and a lower *Calculation* frame. The *View* frame allows to determine and display the first and second derivatives of IRM, COE and RMP curves. Logarithmic scales for the applied magnetic field on the $x$-axis can be selected for IRM and COE. Paramagnetic contributions according to hysteresis measurements can be shown and subtracted from the RMP curve. The *View* frame for HYS curves enables the user to show the para-/diamagnetic corrected hysteresis loop and the hysteresis functions after decomposition (see above). The *Calculation* frame contains options and parameters used for fitting and analyzing the

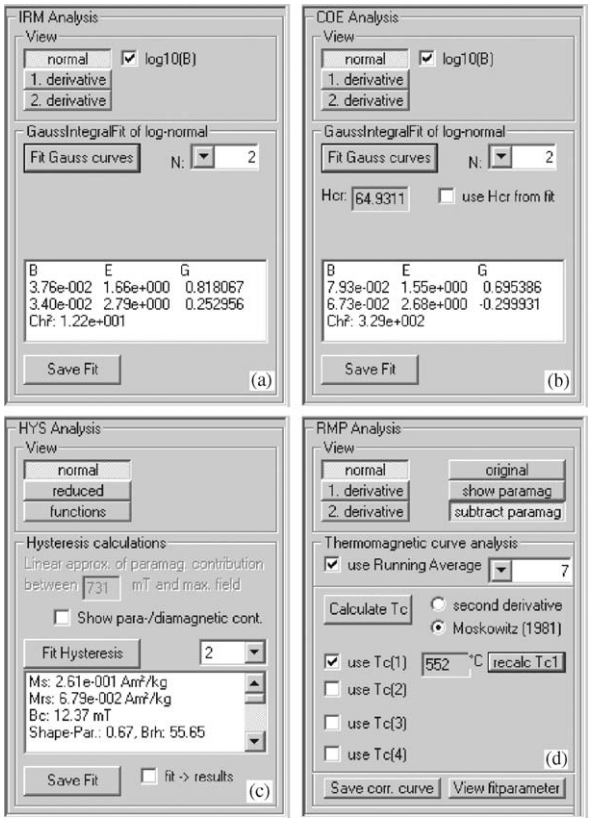


Fig. 3. Insets containing advanced analysis options for: (a) IRM; (b) backfield; (c) hysteresis and (d) thermomagnetic measurements.

measurements. Whether or not parameters obtained from fitted curve should be used for the *Results* field can be selected for COE, HYS and RMP analysis (Fig. 3b–d). A *Save Fit* button is available in all analysis fields. Choosing this option will save the current data fit into a file of VFTB output format.

### 4.1. Data fitting

Advanced analysis data fitting, which is provided by the ROCKMAG ANALYZER is conducted by a standard non-linear least-squares routine, the Levenberg–Marquardt method (Levenberg, 1944; Marquardt, 1963). By fitting a mathematical model to experimental data, unknown parameters in the model are determined. In principle, for a set of initial starting parameters the Levenberg–Marquardt routine optimizes those parameters so that the output of the model is the best match to the observed data. For data fitting of IRM, COE and HYS data up to four cumulative mathematical functions can be fitted to the measured data.

### 4.2. Analysis of IRM and coercivity curves

By using the option *IRM Analysis* or *Backfield Analysis* similar advanced analysis options are enabled. These options allow for fitting the measured data by means of cumulative integrals over log-Gaussian functions. The usage of cumulative log-Gaussian functions to approximate experimental IRM data was suggested earlier (e.g. Robertson and France, 1994; Stockhausen, 1998). In principal, those methods try to find the best fitting cumulative sum of log-Gaussian functions to the first derivative of log-scaled isothermal remanence measurements. Low-field magnetization steps are mostly characterized by the largest slopes and, thus, largest amplitudes of the first derivative. Therefore, least-square fitting of first derivatives leads to a better approximation of low-field steps than of higher field steps. Even more importantly, derivatives of measured data lead to an amplification of noise. In order to avoid such low-field overemphasizing and reduce noise amplification, a slightly different approach is used in the ROCKMAG ANALYZER software.

Plotting e.g. IRM acquisition data (Fig. 4a) linearly versus a log-scaled field axis results in Fig. 4b. This curve is then fitted by using a cumulative sum over integrations of log normal

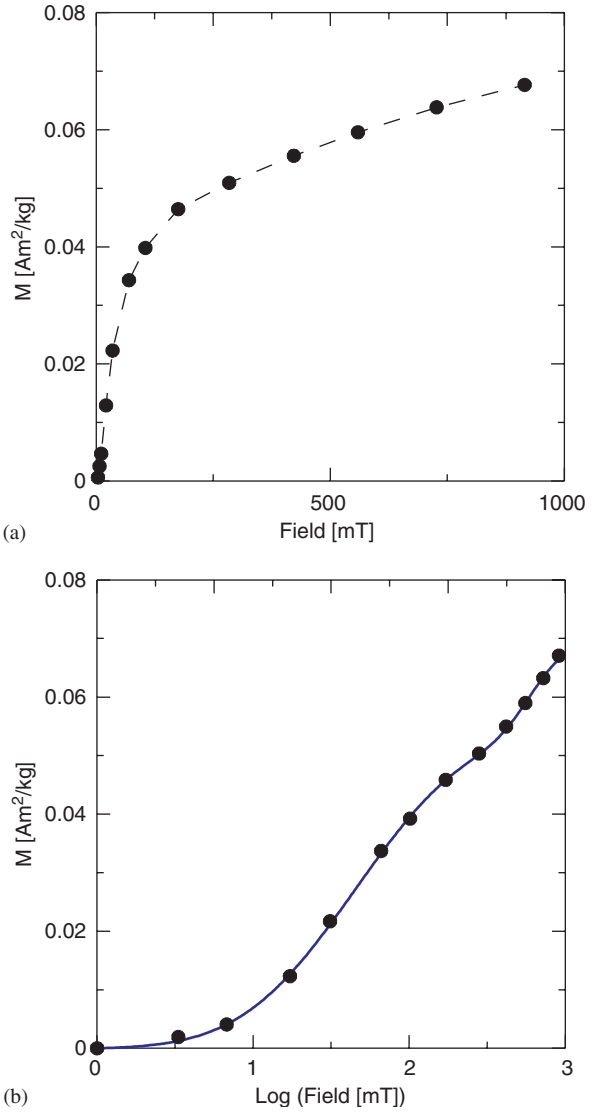


Fig. 4. Fitting of IRM acquisition. (a) Original measured data. In (b) raw data (black symbols) is shown on a logarithmic field scale. Blue line indicates the calculated best fit using sum of two integrals over log-Gauss functions.

Gaussian functions:

$$M_{\mathrm{fit}}(x) = \sum_{i=1}^{N}\left[B_i G_i \frac{\sqrt{\pi}}{2}\left(\mathrm{erf}\left(\frac{x-E_i}{G_i}\right) - \mathrm{erf}\left(\frac{-E_i}{G_i}\right)\right)\right] \quad (3)$$

with $M_{\mathrm{fit}}$ representing the modeled magnetization at the logarithmic field value $x = \log(B)$. $\mathrm{erf}(z)$ is the error function. The cumulative sum of $N \leqslant 4$ functions is determined for parameters $B_i$, $E_i$, and

$G_i$ which describe the log-Gaussian integral function. $E_i$ represents the mean value of a corresponding log-Gaussian distribution, and therefore, the logarithmic field value of the maximum gradient. $G_i$ describes the standard deviation or half-width of the distribution. $E_i$ and $G_i$ are related to the log-Gaussian distribution and, thus, are comparable to the parameters median destructive field ($E_i$) and dispersion ($G_i$) as suggested by Robertson and France (1994). $B_i$ is a weighting factor related to the amplitude of the distribution. These parameters are optimized in the course of the Levenberg–Marquardt routine. Initial start values for the minimization procedure are predefined from the software and were tested on a large data set obtained from a variety of sedimentary and volcanic rocks.

Application of this fitting method to the "example1.irm" data set (Fig. 4a) using $N = 2$ functions results in the modeled blue curve of Fig. 4b. The parameter $\chi^2$, describing the goodness-of-fit between mathematical model and measured data, is also displayed in the parameter field.

### 4.3. Advanced hysteresis analysis

The option *Hysteresis Analysis* allows the user to manually choose the minimum field for the linear fit for para-/diamagnetic slope calculation. This limit has to be chosen at a field strength at which the ferrimagnetic component is saturated. It is possible to show the calculated linear fit in the hysteresis plot. Data fitting of hysteresis loops is supported by means of cumulative coercivity-related hyperbolic basic functions (von Dobeneck, 1996). It has been shown (Stacey and Banerjee, 1974; von Dobeneck, 1996) that hyperbolic tangent functions [$\tanh(x) = (e^x - e^{-x})/(e^x + e^{-x})$] approximate induced hysteretic magnetization. This function is used to fit the mean curve of the hysteresis loop. Hyperbolic secant functions [$\mathrm{sech}(x) = 2/(e^x + e^{-x})$] can fit remanent hysteretic magnetization curves and are used to approximate the difference curve. The implementations of such hyperbolic functions used for the Levenberg–Marquardt routine of the ROCKMAG ANALYZER are:

$$\tanh(z) = \sum_{i=1}^{N} \left( B_i^t \frac{e^{G_i^t z} - e^{-G_i^t z}}{e^{G_i^t z} + e^{-G_i^t z}} \right) + E_1^t z, \quad (4)$$

$$\mathrm{sech}(z) = \sum_{i=1}^{N} \left( B_i^s \frac{2}{e^{G_i^s z} + e^{-G_i^s z}} \right). \quad (5)$$

In Eqs. (4) and (5), $z$ is the applied magnetic field. $B_i^t$ corresponds to the saturation magnetization $M_s$ of component $i$, $G_i^t$ is related to the curvature of the function and, therefore, a measure of the coercivity. $E_1^t$ is the slope of the para-/diamagnetic component and is not optimized by the software. $B_i^s$ is the saturation remanence $M_{rs}$ of component $i$ and $G_i^t$ is again a measure of the coercivity. Beside the standard hysteresis values obtained by using the cumulatively fitted loop, the fit parameters for all $i \leqslant 4$ components are printed to the parameter list box in Fig. 3c. Inserting those parameters in Eq. (4) allows for plotting the functions separately (Fig. 5). Components are composites of a $\tanh(x)$ function and a $\mathrm{sech}(x)$ function, which are characterized by similar coercivity parameters $|G_i|$. Larger values of $|G_i|$ lead to larger slopes of the functions and, therefore, indicate components of lower coercivity. Since saturation is not reached in "example1.hys", hysteresis parameters are likely to be imprecisely estimated. Nevertheless, a low coercive (Fig. 5b) and a high coercive (Fig. 5c) component can be clearly identified after decomposition of the hysteresis loop.

Diagrams of the individual components are available in the hysteresis section of the *Additional plots* field (Fig. 1d).

### 4.4. Thermomagnetic curve analysis

The button *Curve Analysis* enables the advanced analysis options for thermomagnetic curves. Paramagnetic contributions can be shown, as well as subtracted from the curves. The paramagnetic content is obtained from the hysteresis analysis and, therefore, related to the temperature of the hysteresis measurement. Any changes of paramagnetic content in the course of the thermomagnetic measurement e.g. due to alteration is not regarded for. If a paramagnetic contribution is present ($m_p > 0$) subtraction is conducted according to

$$M_{red}(T) = M(T) - m_p B_{RMP} \frac{T_{HYS}}{T}, \quad (6)$$

where $M_{red}$ is the magnetization after reduction of the paramagnetic content, $B_{RMP}$ is the applied field during thermomagnetic curve measurement, and $T_{HYS}$ denotes the temperature during the hysteresis measurement. Units of temperatures are Kelvin. Strong diamagnetic contribution, which are leading to negative $m_p$ and may produce negative magnetizations during thermomagnetic measurements are temperature invariant, thus producing negative

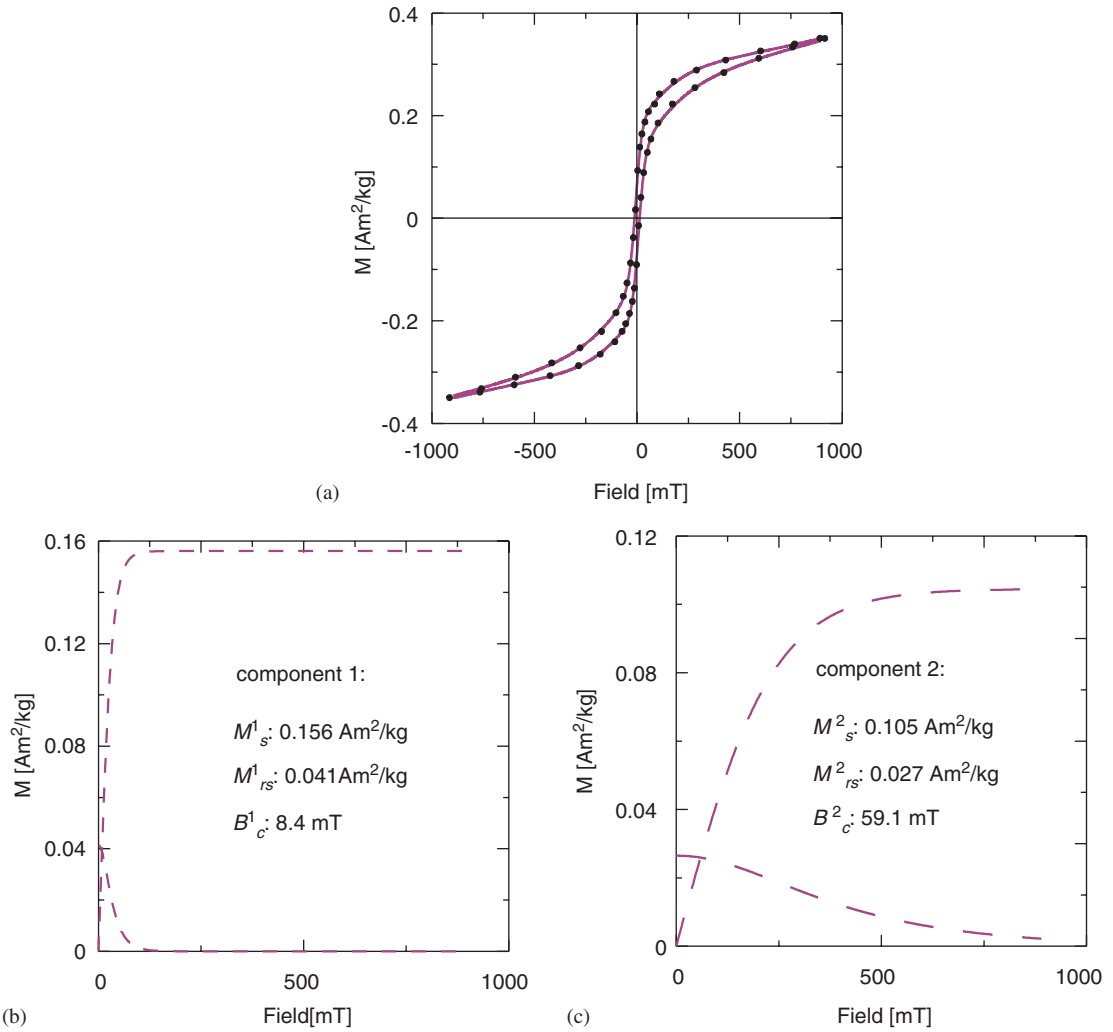


Fig. 5. Hysteresis fit using hyperbolic basic functions. (a) Two tanh($x$) functions, two sech($x$) functions and a linear part are sufficient to obtain a reasonable good fit (purple line) of measured data. Two components identified are plotted separately in (b) and (c), low coercive component in (b) and high coercive component in (c). For interpretation of hysteresis parameters shown in (b) and (c) one has to keep in mind that saturation has not been reached in the experiment.

$y$-offsets of the curve. If negative magnetizations occur in the thermomagnetic curve, the data is automatically shifted up. The amount of the shift, likely representing diamagnetic contribution, is printed to the *Results* field. This reduction is necessary for the correct application of the Moskowitz (1981) Curie temperature estimation approach.

Advanced analysis of thermomagnetic curves focuses on the estimation of Curie temperatures ($T_C$). If the cooling curve is selected, this curve is used for analysis. In the other two cases, the heating curve will be analyzed. Beside $T_C$ calculations, a smoothing option using a running average is supported by the program. The window size for running average can be freely chosen between 3 and 11 data points.

Two different techniques are implemented to obtain $T_C$ from the measured data, the "second derivative approach" and the "Moskowitz (1981) approach" (Fig. 6).

#### 4.4.1. Second derivative approach

The second derivative method relies on the identification of maximum concave curvature within the measured data. The temperature at which this maximum curvature occurs is used as an approximation for $T_C$. Derivatives are calculated by

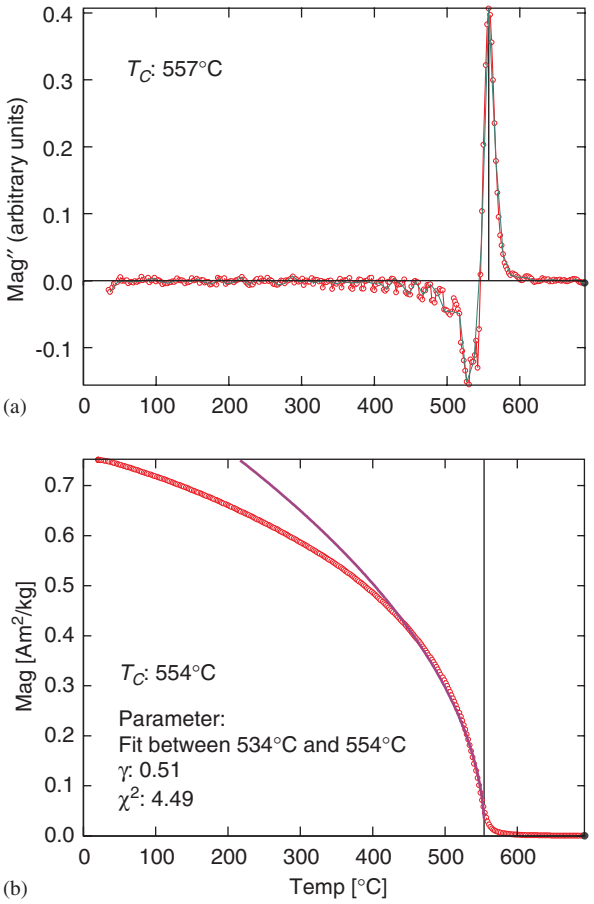


Fig. 6. Two approaches of Curie temperature estimation: (a) $T_C$ determined by the maximum values of the second derivative. Second derivatives are additionally smoothed by a cubic spline function (green line); (b) extrapolation method according to Moskowitz (1981). Black vertical line marks the position of $T_C$ in both plots.

determining the slopes between successive data points of either the raw data or the smoothed curve as defined by the running average. For $T_C$ calculation, both first and second derivatives are further smoothed by cubic splines (Fig. 6a) in order to reduce the noise level. The up to four maximum values of the second derivative, which exceed the remaining noise level of the measurement are used as estimations of $T_C$. The average noise level is determined by a two-sigma standard deviation of the arithmetic average of the second derivative. By choosing the *recalc* $T_C$ option (Fig. 3d) a dialog is opened which allows to select a certain temperature range for $T_C$ calculation. In this case, the temperature value of the maximum of the second derivative within the given temperature range is selected as $T_C$.

#### 4.4.2. Moskowitz (1981) approach

The extrapolation method according to Moskowitz (1981) uses the true temperature dependence of magnetization close to $T_C$. For this approach, first $T_C$'s are determined according to the second derivative approach. Using the obtained values as starting points ($T_C^{start}$), the Levenberg–Marquardt minimization is used to find the best fitting function

$$\frac{M(T)}{M_{lm}} = \left(\frac{T_C}{T_C - T_{lm}} - \frac{T}{T_C - T_{lm}}\right)^{\gamma} \quad (7)$$

for each $T_C^{start}$ (Fig. 6b). In order to satisfy the condition of using temperature steps near $T_C$, the minimum temperature of the fit is set to $T_{lm} \geqslant T_C^{start} - 200\,^{\circ}C$. $M_{lm}$ corresponds to the magnetization at $T_{lm}$. A further condition, which needs to be satisfied is $0.32 \leqslant \gamma \leqslant 0.52$ (Tucker and O'Reilly, 1978). A final, admittedly arbitrary condition, is that at least ten measurement points between $T_{lm}$ and $T_C$ are used for each of the up to four different $T_C$ estimations. In case of manual calculation, a number of restrictions can be defined by the user. Firstly, the $\gamma$ value can be fixed. Secondly, the starting point $T_C^{start}$ can be given and thirdly, the temperature interval for fit calculation can be fixed. Fit parameters, which result from the best fitted model, can be viewed by choosing *View fit parameter* (Fig. 3d).

## 5. Additional plots and their analysis

Choosing the *Additional Plots* option disables the standard *View options* and provides three further selections to plot diagrams of the measured and analyzed data.

### 5.1. Plots based solely on hysteresis parameters

Up to three different additional plots related to hysteresis analysis can be viewed using the option *Hysteresis plots*. The $M_{rs}/M_s$ ratio versus $B_c$ is shown on the upper left of the *View all plots* panel. For possible interpretations of this data see Tauxe et al. (2002). For VSM and AGFM data only, an approach-to-saturation-analysis diagram (Fabian, submitted, 2004) is shown on the upper right. This option is restricted to high resolution data curves since the logarithmic field approximations require a large amount of non-interpolated data points at high field steps. If the hysteresis curve was fitted, the components can be shown separately on the lower left. In this case, also the hysteresis parameters $M_{rs}$,

$M_s$ and $B_c$ are calculated for each component and are displayed in the *Results* box.

### 5.2. IRM and coercivity measurements

Diagrams based on the comparison of IRM acquisition and backfield measurements are shown for the option *IRM/Coercivity plots*. The normalized IRM acquisition curve is plotted versus the normalized backfield curve according to Henkel (1964). Non-interacting SD particles of Stoner–Wohlfarth type (Wohlfarth, 1958) will generate a linear dependency as shown by the red line in Fig. 7. A departure from the ideal line can be caused by interacting single domain assemblages, non-uniaxial asymmetry, or multidomain behavior. In case of magnetic interaction, departures from this line towards the lower part indicate negative magnetic particle interactions. Positive interaction lead to curves above the Stoner–Wohlfarth line. In order to quantify departures from the ideal line, the area between the measured data and the red line is calculated. This parameter ($\Delta E_H$) is added to the *Results* field.

The second plot of option *IRM/Coercivity plots* shows the difference of IRM acquisition and backfield measurement calculated according to

$$\Delta M(B) = \frac{M_{\mathrm{COE}}(B)}{M_{\mathrm{rs}}} - \left(1 - 2\,\frac{M_{\mathrm{IRM}}(B)}{M_{\mathrm{rs}}}\right) \tag{8}$$

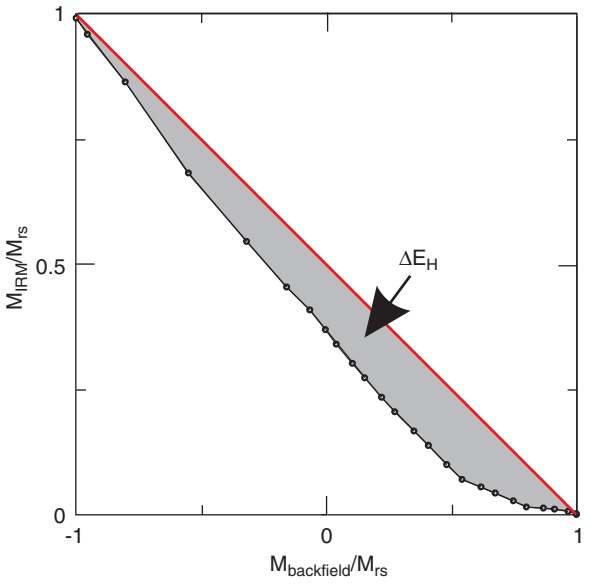


Fig. 7. Analysis of Henkel (1964) plot. Area between measured data and ideal Stoner–Wohlfarth line (red line) is calculated.

versus the applied magnetic field. From this plot the amplitude ($\Delta M_{\mathrm{ex}}$) and the corresponding field of the extremum are determined.

A basic requirement for the analysis of both plots is a remanence acquisition at identical field values for IRM and COE measurements. Since such concordance is typically not the case for VFTB measurements, the IRM data is linearly interpolated. From this interpolated data, magnetization values are determined at field values of the backfield curve.

### 5.3. Domain state estimates

Two additional plots, based on parameters obtained by hysteresis and backfield measurements are provided by selecting *Domain state plots*. Firstly, the classical Day et al. (1977) plot with linear scales of $M_{\mathrm{rs}}/M_{\mathrm{s}}$ versus $B_{\mathrm{cr}}/B_{\mathrm{c}}$ is shown. The second diagram shows the shape parameter $\sigma_{\mathrm{Hys}}$ versus $B_{\mathrm{rh}}/B_{\mathrm{cr}}$ according to Fabian (2003).

## 6. Modification of analysis parameters and view options

In menu *Edit/Options* a number of modifications for data evaluations and view options are provided:

(1) *Backfield curves*: The field at which the S-parameter (Bloemendal et al., 1992) is determined can be changed. The default value is −300 mT.

(2) *Hysteresis loop*: Firstly, the minimum field for determination of the linear slope, and thus, the estimation of the para-/diamagnetic content, can be changed. The default value is 80% of the maximum applied field.
Secondly, the calculation of the parameter $E_t^{\Delta}/E_{\mathrm{Hys}}$ can be enabled. $E_{\mathrm{Hys}}$ corresponds to the total hysteresis area. $E_t^{\Delta}$ is the energy which is dissipated solely by transient irreversible processes (Fabian, 2003). Correct determination of this parameter requires that an initial curve of the hysteresis loop beginning at zero-field is measured from a saturated state ($M_{\mathrm{rs}}$). $E_t^{\Delta}/E_{\mathrm{Hys}}$ determines which fraction of the total energy dissipation is related to the transient energy dissipation (Fabian, 2003). In ideal non-interacting SP/SD mixtures this ratio is zero since no irreversible processes are induced by the self-demagnetizing field. If this option is selected, *Hysteresis/Coercivity plots* in *Additional plots*

shows $\sigma_{Hys}$ versus $E_t^A/E_{Hys}$ instead of $\sigma_{Hys}$ versus $B_{rh}/B_{cr}$.

(3) Additional plots: Values for domain state boundaries in the Day plot can be changed. Domain state boundaries according to Day et al. (1977), Dunlop (2002) or user defined values can be used.

## 7. Discussion and conclusion

The ROCKMAG ANALYZER software provides several different options to analyze rock magnetic measurements. They range from simple to sophisticated methods. The non-standard analysis tools, in particular data fitting by mathematical models, require more discussion.

It has been shown that excellent fits of measured data can be obtained by the software (Figs. 4, 5). The physical significance of the mathematical models and possible interpretations of the obtained parameters, however, need to be discussed in more detail. The primary aim of fitting procedures in the ROCKMAG ANALYZER is to get suitable average curves of noisy data sets. For IRM and backfield measurements, log-Gaussian functions can discriminate between different magnetic phases and, thus, enable an unmixing of ferri-magnetic components (Robertson and France, 1994; Stockhausen, 1998). For a physical explanation for this assumption the reader is referred to Robertson and France (1994). First derivatives of e.g. IRM acquisition curves are thought to be proportional to the coercivity distribution within the sample. Yet, modeling such distributions by log-Gaussian functions is extremely sensitive to measurement uncertainties and to the functions chosen to model the distribution. It has also been shown that such log-Gaussian functions fail to provide suitable fits for interacting magnetic particle assemblages (Heslop et al., 2004). In order to reduce the effect of measurement uncertainties which significantly affect the first derivative, integrals over log-Gaussian functions are used by the ROCKMAG ANALYZER software. The parameters optimized by the software are, however, related to the log-Gaussian distribution and, thus, are comparable at least to the original suggested parameters median destructive field ($E_i$) and dispersion ($G_i$) (Robertson and France, 1994). Other sophisticated approaches towards the modeling of remanence acquisition and demagnetization were suggested for example by Kruiver et al. (2001) and Egli (2003, 2004).

Similar to the procedure of IRM and backfield approximation, the hysteresis analysis by fitting basic hyperbolic functions can be used for the discrimination of coercivity classes. Yet, this technique is only seldom used in rock magnetic studies. Therefore, considerable experimental work is needed in order to determine how rock magnetic properties like domain state, material specific characteristics, etc. translate into hyperbolic functions. A straightforward interpretation of hyperbolic spectra regarding unimodal, bimodal or more complex coercivity distributions related to different magnetic phases cannot be generally drawn.

The Levenberg–Marquardt routine used for data fitting is a very stable and reliable minimization method. However, a 100% success rate of suitable fits cannot be achieved. If the program fails to find a reasonable fit, a message box will inform the user about the failure.

As already stated above, using derivatives in data analysis significantly amplifies measurement noise and may hamper the interpretation. Curie temperature determination using the second derivative approach is significantly affected by such noise amplification. Therefore, spline routines are used to reduce the noise level of the measured data. Furthermore, running averages reduce the measurement noise and often improve the Curie temperature determination. Using the second derivative technique, reasonable estimates for $T_C$, however, can only be obtained if the magnetization is close to zero. $T_C$ will be underestimated in multi-component systems, where a large proportion of magnetization is left after reaching a particular $T_C$. The Moskowitz (1981) extrapolation method should be favored, at least for the analysis of such multiphase samples.

Like most other rock magnetic instruments, the MM VFTB is continually being improved. Future modifications will include AF/ARM capabilities and further modifications. The herein presented software will be updated accordingly. Therefore, the version number 1.0 is assigned to the ROCKMAG ANALYZER.

## Acknowledgements

Nikolai Petersen is acknowledged for his ongoing interest during software development and his constructive comments. I would like to thank

Christoph Heunemann, David Krása and Jürgen Matzka for many helpful discussions. David Dunlop and Richard Ernst provided helpful reviews of the manuscript. Funding was provided by the German Science Foundation (DFG) in the framework of the priority program "Geomagnetic Variations" (So72/67-4).

## References

Bloemendal, J., King, J.W., Hall, F.R., Doh, S.-J., 1992. Rock magnetism of late Neogene and Pleistocene deep-sea sediments: relationship of sediment source, diagenetic processes and sediment lithology. Journal of Geophysical Research 97, 4361–4375.

Day, R., Fuller, M.D., Schmidt, V.A., 1977. Hysteresis properties of titanomagnetites: grain size and composition dependence. Physics of the Earth and Planetary Interiors 13, 260–266.

Dunlop, D., 2002. Theory and application of the Day plot ($M_{rs}/M_s$ versus $H_{cr}/H_c$) 1. Theoretical curves and tests using titanomagnetite data. Journal of Geophysical Research 107 10.1029/2001JB000486.

Egli, R., 2003. Analysis of the field dependence of remanent magnetization curves. Journal of Geophysical Research 102, 2081 doi: 10.1029/2002JB002023.

Egli, R., 2004. Characterization of individual rock magnetic components by analysis of remanence curves, 1. Unmixing natural sediments. Stud. Geophys. Geodaet. 48, 391–446.

Fabian, K., 2003. Some additional parameters to estimate domain state from isothermal magnetization measurements. Earth and Planetary Science Letters 213, 337–345.

Fabian, K., 2004. Approach to saturation analysis of hysteresis measurements in rock magnetism and evidence for stress dominated magnetic anisotropy in young mid-ocean ridge basalt. Physics of the Earth and Planetary Interiors, submitted for publication.

Henkel, O., 1964. Remanenzverhalten und Wechselwirkung in hartmagnetischen Teilchenkollektiven. Physics State Solids 7, 919–929.

Heslop, D., McIntosh, G., Dekkers, M.J., 2004. Using time and temperature dependant Preisach models to investigate the limitations of modeling isothermal remanent magnetization acquisition curves with cumulative log Gaussian functions. Geophysics Journal of Interscience 157, 55–63.

Kruiver, P.P., Dekkers, M.J., Heslop, D., 2001. Quantification of magnetic coercivity components by the analysis of acquisition curves of isothermal remanent magnetisation. Earth and Planetary Science Letters 189, 269–276.

Levenberg, K., 1944. A method for the solution of certain problems in least squares. Quarterly Applied Mathematics 2, 164–168.

Marquardt, D., 1963. An algorithm for least-squares estimation of nonlinear parameters. SIAM Journal of Applied Mathematics 11, 431–441.

Moskowitz, B.M., 1981. Methods for estimating Curie temperatures of titanomagnetites from experimental $J_s$-$T$ data. Earth and Planetary Science Letters 53, 84–88.

Robertson, D.J., France, D.E., 1994. Discrimination of remanence-carrying minerals in mixtures, using isothermal remanent magnetization acquisition curves. Physics of the Earth and Planetary Interiors 82, 223–234.

Stacey, F.D., Banerjee, S.K., 1974. Developments in Solid Earth Geophysics 5: The Physical Principles of Rock Magnetism. Elsevier Scientific Publishing Company, Amsterdam, London, New York.

Stockhausen, H., 1998. Some new aspects for the modelling of isothermal remanent magnetization acquisition curves by cumulative log Gaussian functions. Geophysics Research Letters 25, 2217–2220.

Tauxe, L., Bertram, H.N., Seberino, C., 2002. Physical interpretation of hysteresis loops: micromagnetic modeling of fine particle magnetite. Geochemistry Geophysics Geosystems 10, 1055 doi: 10.1029/2001GC000241.

Tucker, P., O'Reilly, W., 1978. A magnetic study of single-crystal titanomagnetite ($Fe_{2.4}Ti_{0.6}O_4$). Physics of the Earth and Planetary Interiors 16, 183–189.

von Dobeneck, T., 1996. A systematic analysis of natural magnetic mineral assemblages based on modelling hysteresis loops with coercivity-related hyperbolic basic functions. Geophysical Journal International 124, 675–694.

Wohlfarth, E.P., 1958. Relations between different modes of acquisition of the remanent magnetization of ferromagnetic particles. Journal of Applied Physics 29, 595–596.